Hydrothermal synthesis of hexagonal-phase $NaYF_4$: Er, Yb with different shapes for application as photovoltaic up-converters*

Wang Dong-Feng(王东丰)[a], Zhang Xiao-Dan(张晓丹)[a)c)†], Liu Yong-Juan(刘永娟)[b], Wu Chun-Ya(吴春亚)[a], Zhang Cun-Shan(张存善)[b], Wei Chang-Chun(魏长春)[a], and Zhao Ying(赵 颖)[a]

[a] *Institute of Photo-electronics Thin Film Devices and Technique of Nankai University, Key Laboratory of Photo-electronics Thin Film Devices and Technique of Tianjin, Key Laboratory of Photo-electronic Information Science and Technology (Nankai University), Ministry of Education, Tianjin* 300071, *China*

[b] *School of Information Engineering. Hebei University of Technology, Tianjin* 300071, *China*

[c] *State Key Laboratory of Silicon Materials, Zhejiang University, Hangzhou* 310027, *China*

(Received 14 May 2012; revised manuscript received 12 June 2012)

Hexagonal β-$NaYF_4$ co-doped with Yb^{3+} and Er^{3+} is directly synthesized under mild conditions using a hydrothermal method. The variation of the ratio of Ln^{3+} to F^- and ethylenediaminetetraacetic acid (EDTA) causes the shape of the microcrystal to change from microplate to microcolumn. The $NaYF_4$ powder is mixed with polydimethylsiloxane (PDMS) to create an up-converter for thin film amorphous silicon solar cells so as to evaluate the effectiveness of the synthesized material as an up-converter. In order to overcome the difficulty in measuring the effectiveness of up-conversion material, a new method of using near infrared illumination to measure the short circuit current densities of solar cells both with and without up-converters is developed. An up-converter with pure hexagonal $NaYF_4$:Yb^{3+}/Er^{3+} microcrystal produces a high current output. Emission intensity data obtained by photoluminescence suggest that pure hexagonal $NaYF_4$:Yb^{3+}/Er^{3+} microcrystals are more efficient than nanocrystals when used as up-converting phosphors.

Keywords: up-conversion, $NaYF_4$, hydrothermal method, up-convertor, solar cells

PACS: 78.20.–e, 42.65.Ky, 78.55.–m, 42.70.Nq **DOI:** 10.1088/1674-1056/22/2/027801

1. Introduction

As is well known, the solar spectrum covers a very wide range.[1] In particular, in a wavelength range from 200 nm to 2000 nm, the light, such as ultraviolet, visible, and infrared (IR) light, has considerable energy. However, there have been no photovoltaic (PV) devices that can utilize all of the solar energy across this broad spectrum. The main reason for this is the limitation imposed by the band gap of the active layer. Specifically, photons with energies less than the band gap cannot be utilized by solar cells. For example, amorphous silicon thin film solar cells can absorb only photons with wavelengths less than 750 nm. Utilizing more of the solar spectrum is an important issue for the development of high efficiency solar cells.[2]

One solution to this problem is the multi-junction tandem solar cell. In this concept, materials with different band gaps are incorporated into the active layer of solar cells. In these devices, wide band gap materials absorb high energy photons while narrow band gap materials absorb low energy photons.

Another way to solve this problem is to use up-conversion (UC) materials. The UC is an anti-Stokes phenomenon[3] and in principle, UC materials can convert near infrared (NIR) light into visible light which can then be utilized by existing solar cell technology. The limiting efficiency of a PV device that employs luminescent up-conversion of sub-band-gap light has been calculated recently, indicating that a substantial efficiency enhancement (a maximum value of 47.6% for non-concentrated sunlight) can be achieved.[4] The first experimental implementation of up-conversion in GaAs solar cells was reported by Gibart *et al*.[5] in 1995. The first application of an up-converter to a silicon solar cell was reported by Shalav *et al*. in 2003.[6] The use of up-converter materials in solar cells has also been reported in Refs. [7]– [9]. Recently, Chai *et al*.[10] have also done some work on incorporating up-conversion materials into solar cells.

An up-converting material can generate one high-energy photon from every two or more incident low-energy photons. The UC has been studied extensively since the 1960's, and Auzel[11] has written an in-depth review discussing its history, mechanism, and applications. Since the early 1970s, $NaYF_4$:Er^{3+}, Yb^{3+} has been recognized as one of the most efficient NIR-to-visible UC materials.[12–15] Recently, the work on UC materials based on $NaYF_4$ host materials has focused primarily on nanoparticles because particle sizes in the nanometer range are considered necessary for biological imaging.[16,17] However, the low fluorescence efficiency of nanophosphor compared with the fluorescence efficiency of bulk phosphor has restricted its application in solar cells.[18–20]

*Project supported by the National Basic Research Program of China (Grant Nos. 2011CBA00705, 2011CBA00706, and 2011CBA00707), the National Natural Science Foundation of China (Grant No. 60976051), the Science and Technology Support Program of Tianjin, China (Grant No. 12ZCZDGX03600), and the Program for New Century Excellent Talents in University of China (Grant No. NCET-08-0295).

†Corresponding author. E-mail: xdzhang@nankai.edu.cn

© 2013 Chinese Physical Society and IOP Publishing Ltd

In this paper, a hydrothermal method is used to synthesize UC materials. The strong chelating agent ethylenediaminetetraacetic acid (EDTA) is also used to form a complex with lanthanide ions for controlling the growth of the crystals and their sizes. According to the LaMer model[21] the formation of such a complex controls the concentration of lanthanide ions in the solution, and thus helps to control the nucleation and growth of the crystals. In addition, the ratio of Ln^{3+} to F^- is also used to control the shape and crystalline structure of samples. How the NH_4F-to-Ln^{3+} ratio influences the anisotropic growth is analyzed. The $NaYF_4$ powder is mixed with polydimethylsiloxane (PDMS) and then the mixture is applied to thin film amorphous silicon solar cells in order to evaluate the synthesized materials as up-converters using a newly developed technique.

2. Experimental details

$NaYF_4$:Yb, Er phosphors were synthesized as follows: Yb_2O_3 (99.99%) and Er_2O_3 (99.99%) were dissolved in 38% HCl to yield $YbCl_3$ and $ErCl_3$ respectively. YCl_36H_2O and NaCl were dissolved in de-ionized water. As detailed in Table 1, the resulting solutions of YCl_3 (0.2 mol/L), NaCl (0.2 mol/L), $YbCl_3$ (0.2 mol/L), $ErCl_3$ (0.2 mol/L), along with EDTA, were dissolved in ethanol. NH_4F was then added into the solution. Here, it is noted that these particular concentrations of Er and Yb in this series of experiments demonstrated relatively high up-conversion efficiency.[22–24]

Table 1. Experimental parameters for synthesizing samples.

Sample	NaCl/ml	YCl_3/ml	$YbCl_3$/ml	$ErCl_3$/ml	Ethanol/ml	NH_4F/g	EDTA/ml
A	20	16	3.6	0.4	20	0.66672	36
B	20	16	3.6	0.4	20	0.7408	36
C	20	16	3.6	0.4	20	0.88896	36
D	20	16	3.6	0.4	20	1.03712	36
E	20	16	3.6	0.4	20	1.18528	36
F	20	16	3.6	0.4	20	1.33344	36

After vigorous stirring in a 200-ml beaker, the mixture was put into a polytetrafluoroethylene (PTFE) autoclave and heated in an oven for 24 h at 200 °C. The resulting material was extracted by centrifugation. It was then washed three times with ethanol, and then heated in an oven at 100 °C until it became dry powder.

Images of the materials were obtained using scanning electronic microscopy (SEM) with a Jeol JSM-6700F. The XRD spectra were acquired using an advanced X-ray diffractometer (X'pert pro), with CuKα radiation at 1.5405 Å (1 Å = 0.1 nm). The UC fluorescence spectra of the dried powder were measured on an LS-55 (Perkin-Elmer, USA) luminescence spectrometer with an external 980-nm laser diode (400 mW, slit 5 nm) serving as an excitation source. It should be pointed out that the intensity of laser and the size of silt were kept unchanged for all samples during the emission spectra measurement.

3. Results and discussion

3.1. Material properties

$NaYF_4$ exists in two forms of polymorphs at ambient pressure: cubic α-phase and hexagonal β-phase.[25] The cubic $NaYF_4$ is of a fluorite structure ($Fm3m$, $Z = 4$), in which Na^+ and Y^{3+} are randomly distributed among the cationic sites. In the hexagonal phase (space group $P\bar{6}$, $Z = 1$), however, there are three types of the cationic sites: one is fully occupied by Y^{3+}(1a site), the second is randomly occupied by either Y^{3+} or Na^+ (1f site), and the third is fully occupied by Na^+. The hexagonal phase is a thermodynamically stable phase, while the cubic phase is a high temperature metastable phase. Figure 1(a) shows the XRD patterns of $NaYF_4$:Er^{3+}, Yb^{3+} phosphors with different Ln^{3+}-to-F^- molar ratios prepared at 200 °C for 24 h. The diffraction peaks for all of the samples correspond to pure hexagonal $NaYF_4$ with cell parameters $a = 0.598$ nm and $c = 0.35$ nm. Based on the data in Fig. 1(a), it is clear that pure hexagonal $NaYF_4$ can be obtained under wide synthetic conditions and it is shown that the ratio of Ln^{3+} to F^- will change the intensity ratio of (101) to (110). A lower Ln^{3+}-to-F^- ratio results in a higher (110)-to-(101) intensity ratio which is the result of anisotropic growth along the c axis. The details can be seen in Fig. 1(b).

Typical SEM images of the $NaYF_4$ crystals obtained with different Ln^{3+}-to-F^- molar ratios are presented in Fig. 2. Each of the samples exhibits a regular hexagonal microcrystalline shape with diameter and length of the order of microns. In this experiment, higher Ln^{3+}-to-F^-ratios result in hexagonal microcrystals with low aspect ratios (diameter greater than length) while lower Ln^{3+}-to-F^- ratios lead to hexagonal microrods with high aspect ratios (length greater than diameter) as shown in Fig. 2. In our previous research, the fluorescence efficiency of the cubic phase phosphors was at least one order of magnitude less than that of the hexagonal phase.[26] In order to convert the cubic phase into the hexagonal phase and increase the fluorescence, it is necessary to heat treat the

material at 400 °C–600 °C for 5 h which leads to undesirable particle growth and agglomeration as shown in Ref. [27]. From Fig. 2, the experimental results show that pure hexagonal $NaYF_4$ crystals are directly synthesized using a hydrothermal method with ethanol serving as the solvent and EDTA as the chelating agent. Liang *et al*.[28] have also reported on the syntheses of hexagonal $NaYF_4$ crystals with a certain range of aspect ratios depending on ratio of NaF to Y^{3+}. However, their process required a long reaction time (3 days) and complex reaction system (*n*-butanol/water/oleic acid) in comparison with our process which has a short reaction time (1 day) and a simple (ethanol/EDTA acid) reaction system.

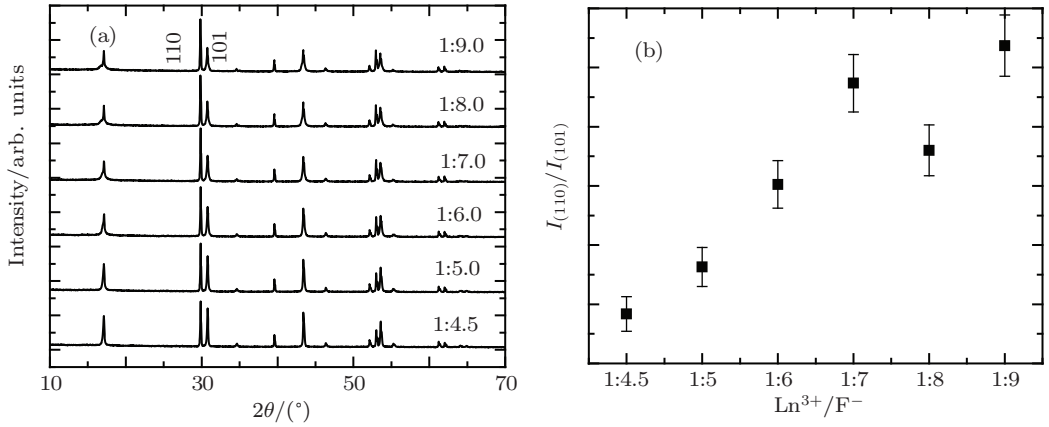


Fig. 1. (a) XRD patterns and (b) $I_{(110)}/I_{(101)}$ of the $NaYF_4$ samples obtained under different ratios of Ln^{3+} to F^- at 200 °C for 24 h.

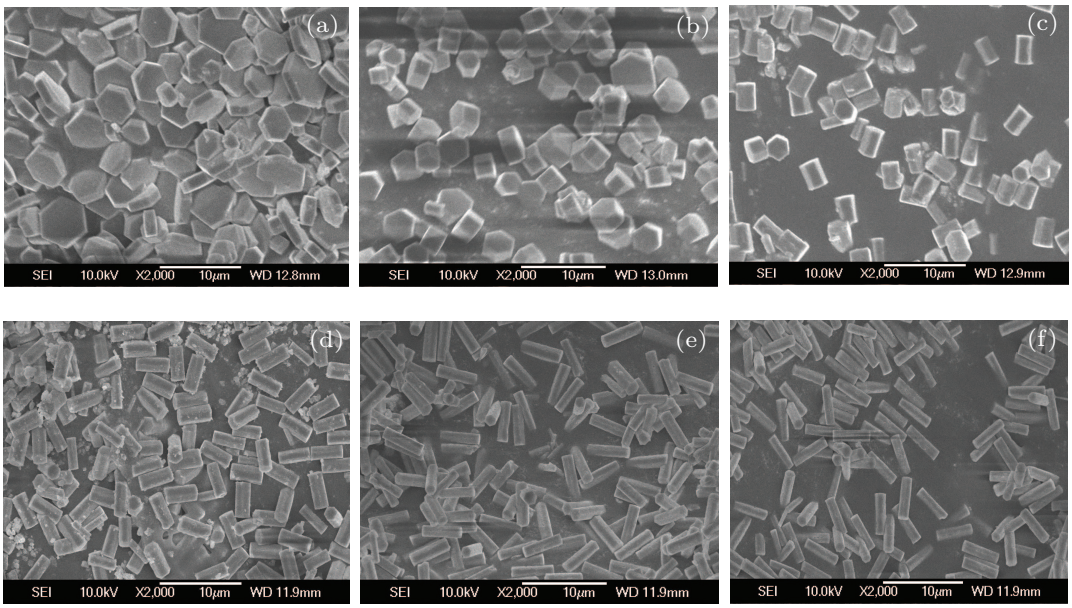


Fig. 2. SEM images of $NaYF_4$: Er^{3+}, Yb^{3+} phosphors with different Ln^{3+}-to-F^- ratios: (a) 1:4.5; (b) 1:5; (c) 1:6; (d) 1:7; (e) 1:8; (f) 1:9 at 200 °C for 24 h.

Table 2. Summary for the sizes of all samples.

Sample	Ln^{3+} / F^-	D/μm	H/μm	D/H
A	1:4.5	6.3	1.0	6.30
B	1:5.0	4.0	2.3	1.74
C	1:6.0	3.0	3.6	0.83
D	1:7.0	1.6	4.0	0.40
E	1:8.0	1.3	5.0	0.26
F	1:9.0	1.3	5.0	0.26

In order to know well the variation in the hexagonal $NaYF_4$ crystals, the particle diameter (D) and height (H) are counted by averaging the corner-to-corner distance of the hexagonal surface and the distance between the top and bottom, respectively. At a high Ln^{3+}-to-F^- molar ratio (Ln^{3+}/F^-=1/4.5), hexagonal crystals with an average corner-to-corner distance of about 6.3 μm and an average height of about 1.0 μm are obtained (Table 2). At a medium Ln^{3+}-to-F^- molar ratio ($Ln^{3+}/F^- = 1/6$), the hexagonal crystals each show a prism-shaped morphology with an L/H ratio close to

unity. At a low Ln^{3+}-to-F^- ratio ($Ln^{3+}/F^- = 1/9$), the samples each take on a long rod-like morphology. The average diameter is about 1.3 μm and the height is about 5.0 μm. It can be concluded that the Ln^{3+}-to-F^- molar ratio has a great influence on the morphology and microstructure of the as-deposited sample. Table 2 summarizes the values of size, D/H, and Ln^{3+}/F^- of all the samples. Similar results were reported by Liang *et al*.[28] and Shan *et al*.,[29] however, the sizes for their samples are different from ours.

While $NaYF_4$ materials doped only with Er^{3+} are considered to be efficient up-converters, especially when compared with other up-converting phosphors,[30] the UC efficiencies of the samples co-doped with Er^{3+} and Yb^{3+} are considerably higher as shown in our previous paper.[22] This is attributed to the very strong absorption cross section of the Yb^{3+} $^2F_{7/2} \rightarrow {}^2F_{5/2}$ transition as compared with that of the $Er^{3+} \rightarrow {}^4I_{15/2} \rightarrow {}^4I_{13/2}$, combined with higher Yb^{3+} concentration than Er^{3+} concentration. The detailed UC mechanism and population processes in Er^{3+} and Yb^{3+} co-doped systems are presented in Fig. 3 which has also been described in Ref. [29]. This energy transfer mechanism for the excitation of the Er^{3+}, Yb^{3+} co-doped sample is described in Ref. [23]. In fact, except emission in the visible range, there is also an emission at around 1.5 μm. For the infrared emission, it may heat solar cells. We deduce that the heat effect is not evident because the temperature coefficient of the silicon thin film is lower than that of bulk-crystalline silicon. However, this is an interesting open issue, and we will continue to pay much more attention to it in future.

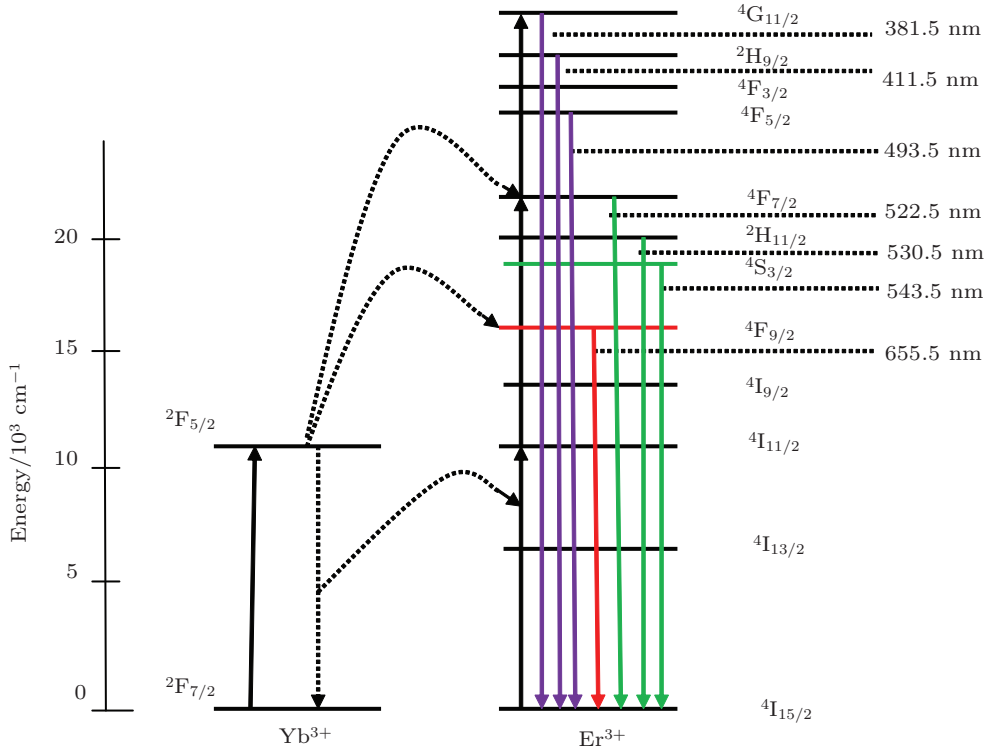


Fig. 3. (color online) Energy-level diagram of Yb^{3+}/ Er^{3+} co-doped UC materials and UC processes under 980-nm excitation.

Room temperature UC fluorescence spectra for $NaYF_4$: Er^{3+}, Yb^{3+} microcrystals are shown in Fig. 4. It is clear that all of the samples show strong emissions in the visible spectral range (400 nm–700 nm) upon NIR excitation (980 nm). Three emission bands centered at 522.5, 543.5, and 655 nm are observed (Fig. 4(b)). The peak around 543.5 nm is the most intense and therefore the UC materials appear bright green when pumped by the 980-nm laser. Furthermore, all of the samples show a strong green-to-red emission ratio. Several factors including doping level, excitation power, and impurity, could influence emission ratio.[31] A much weaker violet emission at 411.5 nm is observed and attributed to the $^2H_{9/2} \rightarrow {}^4I_{15/2}$ electronic transition (Fig. 4(c)).

Green and red luminescence intensity each as a function of the Ln^{3+}-to-F^- ratio are shown in Fig. 5. The UC efficiency decreases with Ln^{3+}-to-F^- ratio decreasing. The variation of UC efficiency can be correlated with the surface properties of the as-deposited sample. Sample B, corresponding to an Ln^{3+}-to-F^- molar ratio of 1:5, produces the highest green intensity.

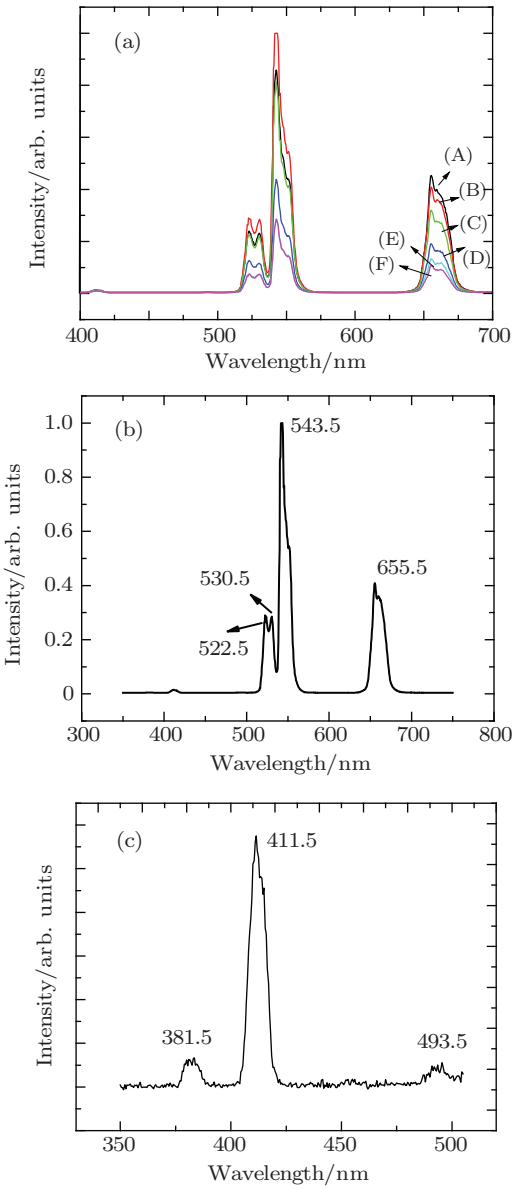


Fig. 4. (color online) (a) Emission spectra of the samples prepared at different Ln^{3+}-to-F^- ratios: 1:4.5 (A), 1:5 (B), 1:6 (C), 1:7 (D), 1:8 (E), and 1:9 (F) at 200 °C for 24 h. The excitation energy is fixed at 400 mW using a 980-nm laser; typical emission spectra in wavelength ranges of 350 nm–750 nm (b) and 350 nm–505 nm (c) of the samples prepared at an Ln^{3+}-to-F^- ratio of 1:4.5 and 200 °C for 24 h.

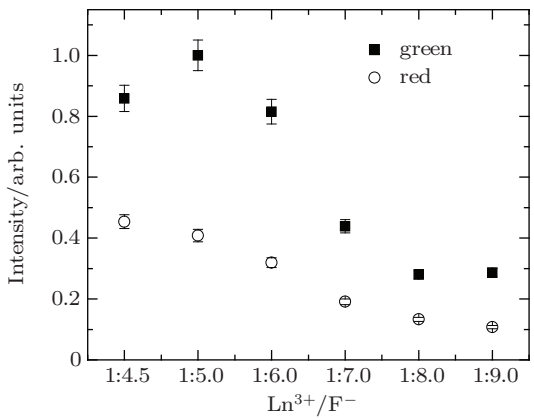


Fig. 5. Green and red luminescence intensity each as a function of Ln^{3+}-to-F^- ratio.

Chen *et al*.[19] reported on a rapid decrease in UC efficiency when the size of Y_2O_2S:Yb, Er nanocrystal decreased from 30 nm to 2 nm. Similarly, figure 6 shows the comparisons of the emission spectrum between $NaYF_4$:Er^{3+}, Yb^{3+} hexagonal microcrystals (sample B) and $NaYF_4$:Er^{3+}, Yb^{3+} hexagonal nanocrystals (corresponding to an Ln^{3+}-to-F^- ratio of 1:4, see Ref. [26]), illustrating that the microcrystals are the more efficient UC materials. The insets show the SEM images of the relevant particles. The decrease in fluorescence efficiency is attributed to the lack of low-frequency phonon modes and restricted excitation migration in the nanoparticles.[19,20] In addition, organic ligands on the surfaces of the nanoparticles quench the ions for fluorescence.[32] Here, it is noticed that compared with the amount of Ln^{3+}, the amount of NH_4F for the sample B (corresponding to an Ln^{3+}-to-F^- ratio of 1:5) exceeds that of the standard reaction condition (corresponding to an Ln^{3+}-to-F^- ratio of 1:4). According to the Gibbs–Thompson theory, the relative chemical potential of a crystal is simply proportional to its surface-to-atom ratio, determined by the average number of dangling bonds per atom over the entire crystal.[29,33,34] In this experiment, excessive F^- ions are inevitably capped on the crystal surface due to the strong coordination effect between Ln^{3+} to F^-. The capping effect of F^- ions can reduce the chemical potential because of the reduction of the average number of dangling bonds. As a result, the chemical potential of the crystal plane varies and then the relative growth rates in different directions change, finally leading to the different crystal morphologies (see the inset in Fig. 6). Similar results and explanation can be found in Ref. [28].

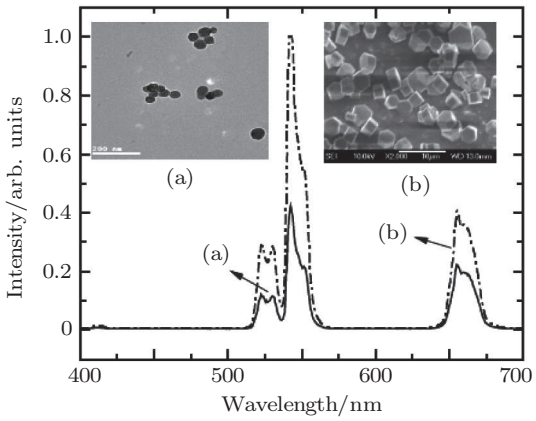


Fig. 6. Emission spectra of nanoparticles with Ln^{3+}-to-F^- ratio of 1:4 (a) and those of microplates with Ln^{3+}-to-F^- of 1:5 (b). The excitation energy is fixed at 400 mW using a 980-nm laser. The insets show SEM images of nanoparticles and microplates respectively.

3.2. Photovoltaic applications

An amorphous silicon thin film solar cell (glass/SnO_2/p/i/n/ZnO/Al) is fabricated by RF-PECVD in order to evaluate the effects of $NaYF_4$:Er^{3+}, Yb^{3+}. The solar cell exhibits a short circuit current density (J_{sc}) of 11.44 mA/cm^2, open circuit voltage (V_{oc}) of 0.912 V, fill

factor (FF) of 70.7%, and efficiency of 7.38% under AM1.5 illumination. Figure 7 shows the external quantum efficiency of the amorphous silicon solar cell. The PV response ranges from 350 nm to 750 nm. When figure 7 is compared with Figs. 4 and 6, it is evident that the present synthesized UC materials, which emit light in a range from 550 nm to 660 nm, are well matched to amorphous silicon solar cells.

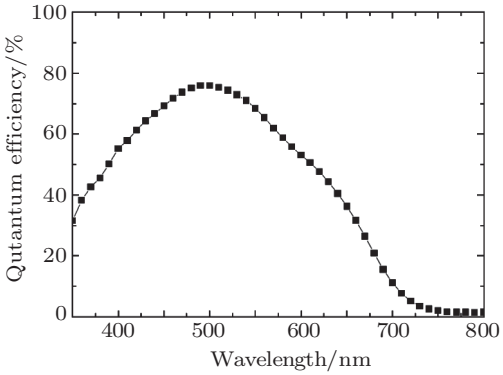


Fig. 7. Curve of quantum efficiency versus wavelength of amorphous silicon thin film solar cell.

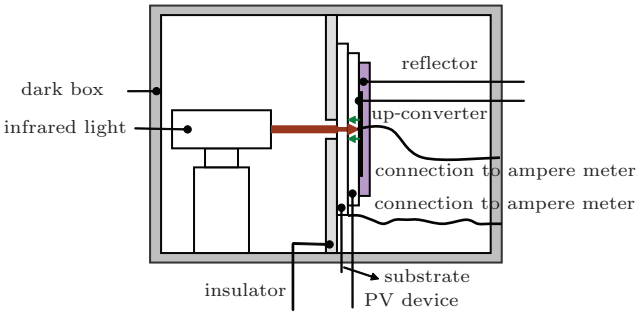


Fig. 8. (color online) Schematic plot of current measurement of PV device with UC material applied to the rear surface.

It is difficult to directly measure the efficiency enhancement induced by UC material in a PV device. The difficulty arises from two sources. The first is the inherent error resulting from the efficiency measurement process. The second is the inhomogeneity of fabricated solar cells. Each of these sources of error reduces the credibility of the measurement of the effectiveness of UC material on the performance of the solar cell.

To solve this problem, a new method of using near infrared illumination to measure the values of short circuit current density (J_{sc}) of solar cells both with and without up-converters is developed. The principle and diagram can be seen in Fig. 8. The samples produced using the hydrothermal method described above are in the powder form and cannot be readily integrated into the active layer of a PV device, especially for a silicon thin film solar cell. Therefore, polydimethyl–siloxane (PDMS) is mixed with the above powder to create an up-converter paste. The UC material is applied to the rear side of an amorphous silicon solar cell. In a dark box, the solar cell is illuminated with an IR light source. In our experiment, a 980-nm NIR laser is used as a light source. The IR light goes through the solar cell and reaches UC material which then converts low energy (IR) photons into high energy (visible) photons. These high energy photons are reflected by a reflecting surface and then absorbed by the solar cell. Any resulting current is measured using an ammeter. The current is then divided by the area of the solar cell to determine the short circuit current density. As detailed in Table 3, up-converters with different shapes and in different concentrations are evaluated for amorphous silicon thin film solar cells. The basic structure of the amorphous solar cells is glass/SnO_2/p/i/n/ZnO. It is noticed that two selected amorphous silicon solar cells are used to characterize the effect of the up-convertor. The diameter of the laser light is 0.5 cm which determines the active area of the solar cell. For the solar cell with no UC layer, no current is generated. From the table, it can be seen that microcrystalline material that includes microplates and microrods yields a higher output than nanoparticle material in this paper. This is in agreement with the emission data described above. Further, microplates also yield higher current than microrods which is also consistent with the high green light shown in Fig. 5. As is well known, the amorphous silicon solar cell has higher absorption around 550 nm. In addition, a higher concentration of UC material yields a higher current output.

Table 3. Applications of up-convertors with different size shapes and different mass densities.

UC sample	0		0.01 g/cm^2		0.02 g/cm^2		0.03 g/cm^2	
Cell sample	1#	2#	1#	2#	1#	2#	1#	2#
Nanoparticle J/mA·cm^2	0	0	0.015	0.015	0.018	0.017	0.02	0.02
Microplate J/mA·cm^2	0	0	0.082	0.081	0.102	0.102	0.122	0.122
Microrod J/mA·cm^2	0	0	0.079	0.078	0.099	0.098	0.11	0.109

4. Conclusions

A hydrothermal method is successfully used to prepare $NaYF_4$ co-doped with Er^{3+} and Yb^{3+} at 200 °C for 24 h. XRD and SEM data show that pure hexagonal microcrystalline materials are directly synthesized by using ethanol as the solvent, EDTA as the chelating agent and by varying the ratio of Ln^{3+} to F^-. The emissions of green and red visible light obtained under the excitation with a 980-nm laser indicate that these UC phosphors have great potential applications in solar cells. In addition, to overcome the difficulty in measuring the effec-

tiveness of UC materials in photovoltaics, a new method of using near infrared illumination to measure the short circuit current densities of solar cells both with and without an up-converter is developed. The results show that high current can be produced if $NaYF_4$:Er^{3+}, Yb^{3+} UC phosphor is applied to an amorphous silicon thin film solar cell.

References

[1] Liu En-Ke 1980 *Photovoltaic Cell Devices and Its Application* (Beijing: Science Press)

[2] Trupke T, Shalav A, Richards B S, Würfel P and Green M A 2006 *Sol. Energy Mater. Sol. Cells* **90** 3327

[3] Tropper A C, Carter J N, Lauder R D T, Hanna D C, Davey S T and Szebesta D 1994 *J. Opt. Soc. Am.* B **11** 886

[4] Trupke T, Green M A and Würfel P 2002 *J. Appl. Phys.* **92** 4117

[5] Gibart P, Auzel F, Guillaume J C and Zahraman K 1995 13th *EPVSEC*, Nice, France, p. 85

[6] Shalav A, Richards B, Trupke T, Corkish R, Krāmer K, Gūdel H and Green M 2003 *Third Conference on Photovoltaic Energy Conversion*, Osaka, Japan, p. 248

[7] Liu M, Lu Y L, Xie Z B and Chow G M 2011 *Sol. Energy Mater. Sol. Cells* **95** 800

[8] de Wild J, Rath J K, Meijerink A, van Sark W G J H M and Schropp R E I 2010 *Sol. Energy Mater. Sol. Cells* **94** 2395

[9] Shalav A, Richards B, Trupke T, Krāmer K W and Güdel H U 2005 *Appl. Phys. Lett.* **86** 013505

[10] Chai R T, Lian H Z, Hou Z Y, Zhang C M, Peng C and Lin J 2010 *J. Phys. Chem.* C **114** 610

[11] Auzel F 2004 *Chem. Rev.* (Washington, D. C). **104** 139

[12] Menyuk N, Dwight K and Pierce J W 1972 *Appl. Phys. Lett.* **21** 159

[13] Kano T, Yamamoto H and Otomo Y 1972 *J. Electrochem. Soc.* **119** 1561

[14] Bril A, Sommerdijk J L and De Jager A W 1975 *J. Electrochem. Soc.* **122** 660

[15] Sommerdijk J L 1973 *J. Lumin.* **6** 61

[16] Li Z Q and Zhang Y 2006 *Angew. Chem. Int. Ed.* **45** 7732

[17] Yi G S and Chow G M 2006 *Adv. Funct. Mater.* **16** 2324

[18] Liu G K, Zhuang H Z and Chen X Y 2002 *Nano Lett.* **2** 535

[19] Chen X Y, Zhuang H Z, Liu G K, Li S and Nidbala R S 2003 *J. Appl. Phys.* **94** 5559

[20] Liu G K, Chen X Y, Zhuang H Z, Li S and Niedbala R S 2003 *J. Solid State Chem.* **171** 123

[21] Lamer Victor K and Robert H D 1950 *J. Am. Chem. Soc.* **72** 4847

[22] Jin X, Zhang X D, Lei Z F, Xiong S Z, Song F and Zhao Y 2008 *Acta Phys. Sin.* **57** 4580 (in Chinese)

[23] Suyver J F, Grimm J, Krāmer K and Güdel H U 2005 *J. Lumin.* **114** 53

[24] Wang F, Chatterjee D K, Li Z Q, Zhang Y, Fan X P and Wang M Q 2006 *Nanotechnology* **17** 5786

[25] Mai H X, Zhang Y W, Si R, Yan Z G, Sun J D, You L P and Yan C H 2006 *J. Am. Chem. Soc.* **128** 6426

[26] Zhang X D, Jin X, Wang D F, Xiong S Z, Geng X H and Zhao Y 2010 *Phys. Status Solidi* C **7** 1128

[27] Yi G S, Lu H C, Zhao S Y, Yue G, Yang W J, Chen D P and Guo L H 2004 *Nano Lett.* **4** 2191

[28] Liang X, Wang X, Zhuang J, Peng Q and Li Y D 2007 *Adv. Funct. Mater.* **17** 2757

[29] Shan J N, Uddi M, Wei R, Yao N and Ju Y G 2010 *J. Phys. Chem.* C **114** 2452

[30] Auzel F and Pecile D 1973 *J. Lumin.* **8** 32

[31] Krāmer K W, Biner D, Frei G, Güdel H U, Hehlen M P and Lüthi S R 2004 *Chem. Mater.* **16** 1244

[32] Heer S, Lehmann O, Hasse M and Gudel H U 2003 *Angew. Chem. Int. Ed.* **42** 3179

[33] Yan R X, Sun X M, Wang X, Peng Q and Yi Y D 2005 *Chem. Eur. J.* **11** 2183

[34] Yu S H, Liu B, Mo S M, Huang J H, Liu X M and Qian Y T 2003 *Adv. Funct. Mater.* **13** 639